

Advanced Biaxial Cruciform Testing at the NIST Center for Automotive Lightweighting

Mark A. Iadicola, Adam A. Creuziger, and Tim Foecke
Materials Sciences and Engineering Division
National Institute of Standards and Technology
Gaithersburg, MD, USA

ABSTRACT

Modeling of sheet metal forming operations requires mechanical properties data at very large tensile strains and various biaxial strain paths. Typically these data are developed along strain ratio paths that are linear and monotonic, but actual forming strain paths are nonlinear and not necessarily monotonically increasing. A unique planar-biaxial testing facility at the National Institute of Standards and Technology (NIST) has been designed to address non-linear strain paths and other long standing measurement needs. The system uses a combination of four independently controlled hydraulic actuators, with either displacement, force, or strain feed back control, to deform the material, while measurements of the material response is accomplished through a unique combination of digital image correlation and X-ray diffraction. Results of commissioning tests are presented for displacement and force control along different axes. The system was able to deform the sample in the elastic and plastic regimes. The results show the difference between the displacement and strain paths followed, as well as some unexpected behavior (e.g. buckling). Other expanded system capabilities for future use are briefly described.

KEYWORDS: biaxial deformation; cruciform; digital image correlation; X-ray diffraction; infrared imaging

1.0 Introduction

The drive for improved fuel efficiency is pushing the auto industry to remove weight from their entire vehicle fleet. A major target for this lightweighting is the sheet metal components (e.g. unibody frame, doors, hoods, deck lids, and fenders). One method to achieve these goals is moving to advanced high-strength or lower density sheet metals, but designers need more robust material models for these materials to make full use of their potential. The more robust models must be calibrated through the entire forming strain range (plastic strains often > 0.20 m/m) and complex strain paths (e.g. plane-strain followed by uniaxial transverse deformation). Classic models calibrated using simple uniaxial tests are not sufficient to capture the evolving material properties during complex and/or multistage forming processes. More complex models require more complex data for calibration. These data often are developed through bilinear strain paths, where samples are strained in a first stage, unloaded, machined, and then deformed through a second linear strain path. The possible effects of unloading and machining include changes in the material response. Biaxial deformation is occasionally used, but typically is performed over a single linear strain path, especially for tests to very high strains (e.g. bulge testing). Cross-shaped (cruciform) biaxial testing could be used to perform some nonlinear strain paths without unloading, but currently is typically used for linear strain paths and still suffers from biaxial failure at strains (typically < 0.05 m/m) well below the forming limits (strains ≈ 0.30 m/m) for the same material [12]. These tests also require modeling (that assumes a constitutive law) to relate the applied loads to the stress and strains in the gauge section.

To address these and other long standing issues the National Institute of Standards and Technology Center for Automotive Lightweighting (<http://www.nist.gov/lightweighting/>) in Gaithersburg, MD has developed an advanced biaxial testing facility over the last few years which uses a unique combination measurement systems integrated into a high capacity biaxial testing machine. The facility is designed to test cross-

shaped high strength sheet metal samples, although other shapes and materials can be tested. The overall system is designed to permit large biaxial strain through controlled non-linear and non-monotonic strain paths without unloading the sample. The mechanical testing machine can run a static test in load, displacement, or strain control, or any logical combination of these methods, on each axis. The strain control and measurement is achieved through a combination of non-contacting two-dimensional (2D) real-time and three-dimensional (3D) post-processed digital image correlation (DIC) systems. An X-ray diffraction (XRD) method similar to [5,9] is used to determine the surface biaxial stress state through measurement and analysis of the crystal lattice strains at a spot in the specimen gauge section. Optional non-contacting measurement of surface temperature can be performed using a 2D infrared (IR) imaging camera system. This paper describes the facility's basic mechanical testing capabilities (using force and displacement control) for one candidate specimen shape, and presents the results from some of the commissioning testing. The additional strain control and other measurement systems will be described in a general way with the details left for future work.

2.0 Facility Description

The biaxial cruciform mechanical testing machine is oriented horizontally (Fig. 1a) with the surface of the specimen level and about 1.5 m (5 ft) above the laboratory floor. The XRD and 3D-DIC systems are attached to the machine frame above the specimen, and the IR camera and 2D-DIC systems are attached to the machine frame below the specimen (Fig. 1b). The 3D-DIC and IR systems could be repositioned without loss of functionality, but when the 2D-DIC system is used for strain control the system must have clear line-of-sight of the specimen gauge section. The XRD system is hung from a moveable gantry frame, and when XRD measurements are required the gantry is positioned directly above the specimen (Fig. 1a). In this paper, we will only discuss the basic mechanical testing system and 3D-DIC measurement systems. Details of the other systems (i.e. 2D-DIC, infrared imaging, and X-ray diffraction) will be discussed in a future paper.

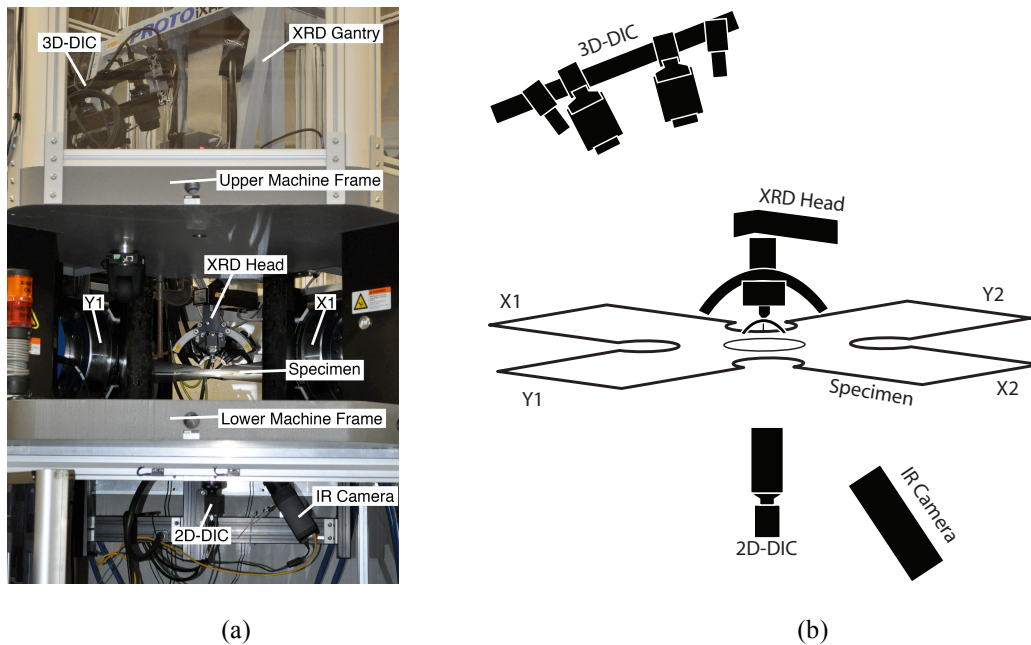


Fig. 1 (a) Annotated photograph and (b) schematic representation of the cruciform specimen, various measurement systems, and actuator positions (X1, X2, Y1, and Y2).

2.1 Mechanical System

The mechanical testing system is based on four independently controlled hydraulic actuators (X1, X2, Y1, and Y2 shown in Fig. 1) aligned in orthogonal pairs (X-axis and Y-axis). Each actuator has a ± 500 kN load capacity, and has a ± 50 mm displacement range from a reference distance of 640 mm between grip faces on

each axis. Control feedback signals include: displacement position from four linear variable differential transformers (LVDTs) and load from four load cells, one for each actuator. The actuators can be programmed individually or in pairs using various combinations of these control signals. For cruciform testing, the actuators are typically controlled in axis pairs (matrix mode). In matrix mode, each axis displacement is the sum of the actuator displacement for each pair (positive tension and negative compression resulting in a total range of ± 100 mm), and the difference between the displacements for each axis is an offset displacement (e.g. negative toward X1 and positive toward X2). The load in matrix mode is reported as the average between each actuator in the pair (positive tension and negative compression), and the difference between the loads on each pair of actuators along an axis is reported as an offset force for that axis. For cruciform shaped samples, the offset force is typically controlled to zero to prevent shearing of the specimen arms on the orthogonal axis. The system allows the specific signal used for control during a test to be changed without unloading the specimen (e.g. load control to a given displacement followed immediately by displacement control to an additional amount of force), but does not allow a switch from matrix mode to independent actuator control while under load. The control modes are also axis independent allowing one axis to be controlled by one signal while the other is controlled by a different signal (e.g. simultaneous load control on X-axis and displacement control on the Y-axis). Care must be taken in programming a logical loading sequence that does not result in an unstable and uncontrollable situation. A classic example is the use of displacement control during compression testing where buckling may occur, as opposed to using load control that can become unstable if buckling occurs. The designed maximum loading rates for matrix mode control are 50 kN/s in force control and 20 mm/s at maximum force in displacement control.

2.2 Digital Image Correlation

Digital image correlation analysis measures the motion of a high contrast pattern on the surface of a specimen [16]. This can be accomplished with a single camera to measure the 2D displacement of a flat surface, or using a multi-camera system to measure the 3D shape and motion of a flat or curved surface. The cruciform facility has three DIC systems: one real-time 2D-DIC for control feedback (not used in the examples shown here) and two full-field 3D-DIC systems to measure strains in the gauge section and loading tabs that require post-processing analyses.

Each of the 3D-DIC systems uses a pair of Point Grey GRAS-50S5M-C five mega pixel CCD cameras viewing the specimen surface from a slightly oblique angle (Fig. 1). One system views only the middle 50 mm by 50 mm of the gauge area (using a pair of Sigma 105mm f/2.8 EX DG telephoto macro lenses), while the other has a field of view approximately 200 mm by 200 mm (using a pair of Schneider-Kreuzach Xenoplan 1.9/35-0901 compact lenses) to monitor the end tabs extending from the gauge area. In this way, the strain response of both the global (overall view) and local (center of the gauge section) areas of the specimen are measured on the top of the specimen independent of the 2D-DIC strain control monitored on the bottom surface (Fig. 1). The 3D-DIC cameras have a maximum frame rate of 5 Hz at full resolution. An estimate of the noise and systematic errors can be made using an analysis of the undeformed pattern as imaged by this camera system configuration. Based on this analysis the total uncertainty (assuming \pm one standard deviation) is $\pm 140 \times 10^{-6}$ strain and $\pm 280 \times 10^{-6}$ strain for the global and local systems, respectively. Engineering strain (ϵ) is used throughout this paper, but other strain measures could be used as well.

2.3 Data Acquisition and Synchronization

Since each system is running almost completely independent of the other systems, synchronization of the data can be a challenge. The mechanical testing system can acquire the control and feedback signals during procedures for later analysis. There is also the ability to acquire more external signals (digital or analog). The 3D-DIC system can acquire up to eight analog signals simultaneously with the image acquisition, which are selected here to record force and displacement signals from the mechanical testing system.

2.4 Other Measurement Systems

In order to follow a realistic non-linear strain path, accurate strain control will be required. A two-axis contact extensometer measurement was attempted, but resulted in premature failure due to specimen damage caused by the extensometer's point contacts. Various non-contact strain measurement methods were considered, and a 2D-DIC system was determined to balance the needs for accurate real-time high-

strain measurement and ease of use. This system has recently been added below the specimen (Fig. 1). An X-ray diffraction system is mounted above the specimen (Fig. 1), and is designed to serve multiple purposes. The first is to be used to measure the interatomic lattice strain to estimate the stress at a point using the " $\sin^2\psi$ " method [14], similar to [5,9], but for cruciform specimens rather than forming limit specimens. The system shown in Fig. 1 has two detector pairs that permit measurement of two different reflections. These could be used to measure two phases in the same sample simultaneously, and may be used to determine the load partitioning between multiple phases. Another potential use for the XRD system is to monitor the amount of phase transformation seen in particular alloys during plastic deformation (e.g. transformation induced plasticity, TRIP, steels). An infrared camera has been added below the specimen for use monitoring adiabatic heating during plastic deformation or phase transformations. This system could also be used for during elevated temperature testing. Detailed descriptions and testing of these systems will be included in a future paper.

3 Biaxial Specimen Design

The use of cruciform shaped specimens to determine the biaxial mechanical properties of sheet metal material is quite common [15,4,8,12,6], but the exact design of the specimen varies widely [13,11,17,7,10,2,1]. Most designs try to develop a uniform strain region in the gauge section for simple linear strain paths. This is done through either adding reentrant radii at the meeting point of the arms (Fig. 2a), or constraint relief slits in the arms (Fig. 2b), or a combination of both. Finite element analyses are typically used to optimize on a basic design with some success, and these same analyses are needed to estimate the stress in the gauge section based upon the load imposed on the arms and an assumed constitutive law. These specimen geometries invariably fail outside the center gauge section at strains well below the biaxial forming limit strains, due to inevitable stress and deformation concentrations in the corners or near the slits in the arms. In some designs, the center of the gauge section is machined to a thinner cross-section (Fig. 2c) to achieve higher strains or even failure in the middle of the gauge area. Although this is less desirable than using the as-received sheet, it is a reasonable starting point for specimen design. In this paper, the specimens use a geometry similar to [1], but enlarged in the plane of the specimen (Fig. 3). [1] reported achieving failure in the center of the gauge section for heated specimens. The results of our testing show that this simple scaling in the plane of testing was not sufficient to force failure in the middle of the gauge area (see Section 4), but did permit the basic commissioning testing of our biaxial cruciform system. The specimen as designed in Fig. 3 was able to achieve plastic strains in the gauge area, but was also susceptible to buckling along some loading paths.

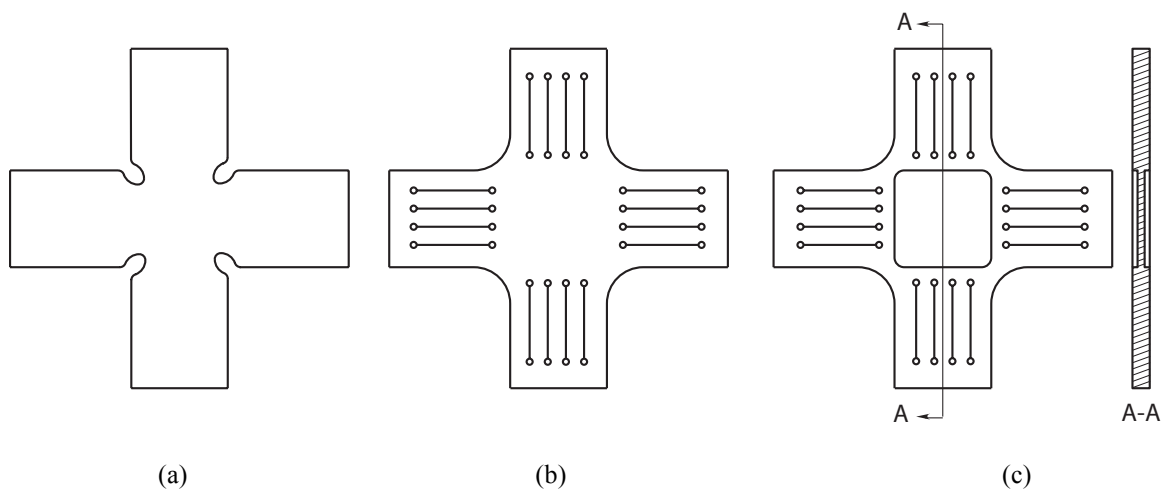


Fig. 2 Cruciform specimen design themes commonly seen in the literature: (a) reentrant corners, (b) relief slits in the arms, and (c) reduced thickness in the gauge area.

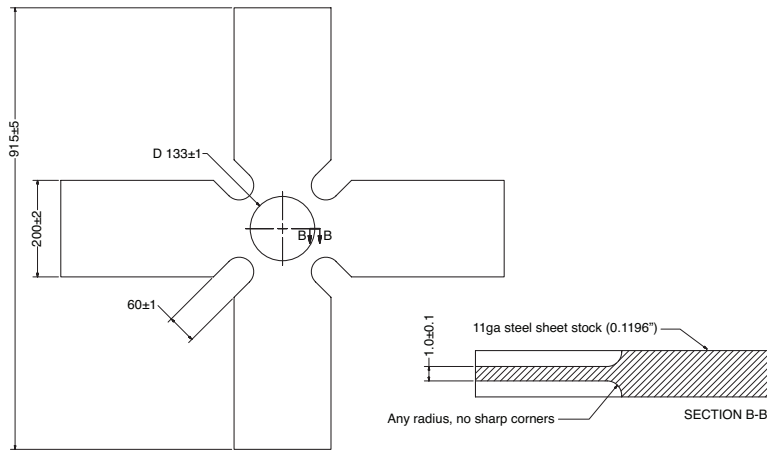


Fig. 3 Cruciform geometry used in examples shown here (dimensions in mm).

4 Results

A series of tests were performed to verify the capacity, control, and measurement systems of the new facility. The results presented here are a small portion of those tests, and demonstrate just some of the systems capabilities. Examples 1 and 2 are cruciform tests performed exclusively in force or displacement control along simple paths. The 2D-DIC system for strain control was not yet installed at the time of these tests. For both examples shown here, the system control was in matrix-mode with the offset force on each axis set to 0 kN. In Example 1, the strains were intended to be limited to the elastic regime, but some small plastic straining (residual strain when unloaded) did occur near the end of the test. In Example 2, strains well into the plastic regime were intended, but resulted in nonlinear buckling behavior. No buckling was seen in Example 1.

4.1 Example 1: Force and Displacement Control in the Low Strain Regime

In this example, a mild steel sample machined to the specimen geometry shown in Fig. 3 is used. The intention of this test was to verify the displacement and force control in the elastic regime, but some plastic deformation did occur. Figures 4a, b, and c show the resulting paths followed in displacement, force, and strain space, respectively. This is the data acquired by the 3D-DIC system, and the strain measured by analyzing the images including the specimen loading tabs. Each path has key points labeled A through I where control paths were changed. The arrows show the direction of time increasing along each segment of the path, and the matrix control mode is noted as "dc" for displacement control and "fc" for force control (strain control is not used in this example). For this example the control mode was applied to both axes, which is denoted by the "XY" label for each control mode (Fig. 4). Force offset control is used on both axes and set to 0 kN. Equi-biaxial force control is demonstrated on segment A-B, where as equi-biaxial displacement control is demonstrated on segment D-E. Segments B-C and C-D demonstrate displacement control resulting in behavior between the uniaxial and equi-biaxial strain conditions. At the end of segment C-D, there is a four minute pause when the system was placed in manual control and unloaded slightly to balance the forces between the axes before the equi-biaxial unloading segment D-E. Uniaxial force control (not to be confused with uniaxial deformation) is demonstrated in segments E-F-G in the X-direction and G-H-I in the Y-direction, where the transverse force is held near zero in each case. During these segments plastic deformation occurred. The results of the plastic deformation can be seen at point G (at zero force) where there is a residual strain, and similarly for point I (at zero force) where there is a residual strain. It is interesting to note that segments E-F-G and G-H-I that exhibit plastic deformation do not exceed the load levels for segments A through E where no residual strain was seen (Fig. 4b). This example also demonstrates an important point in understanding cruciform testing, which is that even in the elastic range (A through E) the shape of the paths are not identical in displacement (Fig. 4a) and strain space (Fig. 4b), thus the grip/arm displacement ratio does not indicate the applied strain ratio in the gauge section even for elastic deformation.

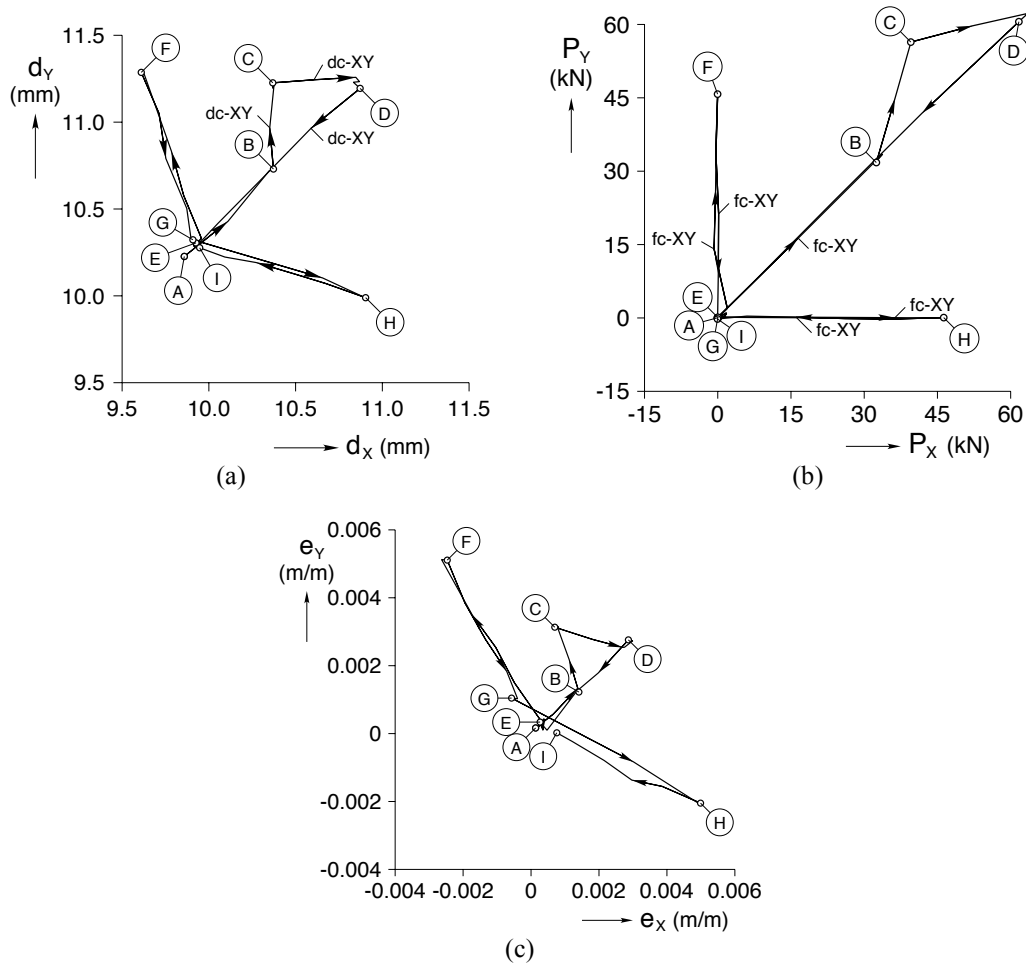


Fig. 4 Results for Example 1 (a) displacement, d , (b) force, P , and (c) strain, e , along the specimen X and Y axes. Key points in the loading paths are labeled by letters A through I, and the progression is denoted by the arrow on each segment. "dc" denotes displacement control and "fc" denotes force control, with suffix "X" is applied to the X-axis and "Y" if applied to the Y-axis. Uncertainties in displacement and force are on the order of the line thicknesses shown in (a) and (b), and in strain are ± 0.00014 m/m.

4.2 Example 2: Combined Force and Displacement Control in the Plastic Regime

Example 2 uses the same specimen as Example 1, but deforms the sample well into the plastic regime. This example also combines the control modes in each segment such that one axis might be in displacement control while the other is in force control. Figures 5a, b, and c plot the resulting paths in displacement, force, and strain space, respectively, similar to Fig. 4 for Example 1. Again, key points are labeled with letters A through J where the control paths were changed, and arrows show the direction along these paths. The matrix control modes are still shown as "dc" and "fc" for displacement and force, respectively, but "X" and/or "Y" are added to show to which axis this is applied. For example, segment B-C labeled "fc-XY" is performed in force control along both axes, where as segment A-B labeled "dc-Y" and "fc-X" is performed in displacement control along the Y-axis with simultaneous force control along the X-axis. Again, the offset force is set to 0 kN along both axes. Since this is the same specimen as Example 1, point A is located at the same displacement, force, and strain as the end point (I) in Example 1. Note that the residual strain after Example 1 (I in Fig. 4c) is not as visible at the initial point in Fig. 5c because the axis range is much larger in Fig. 5c than in Fig. 4c.

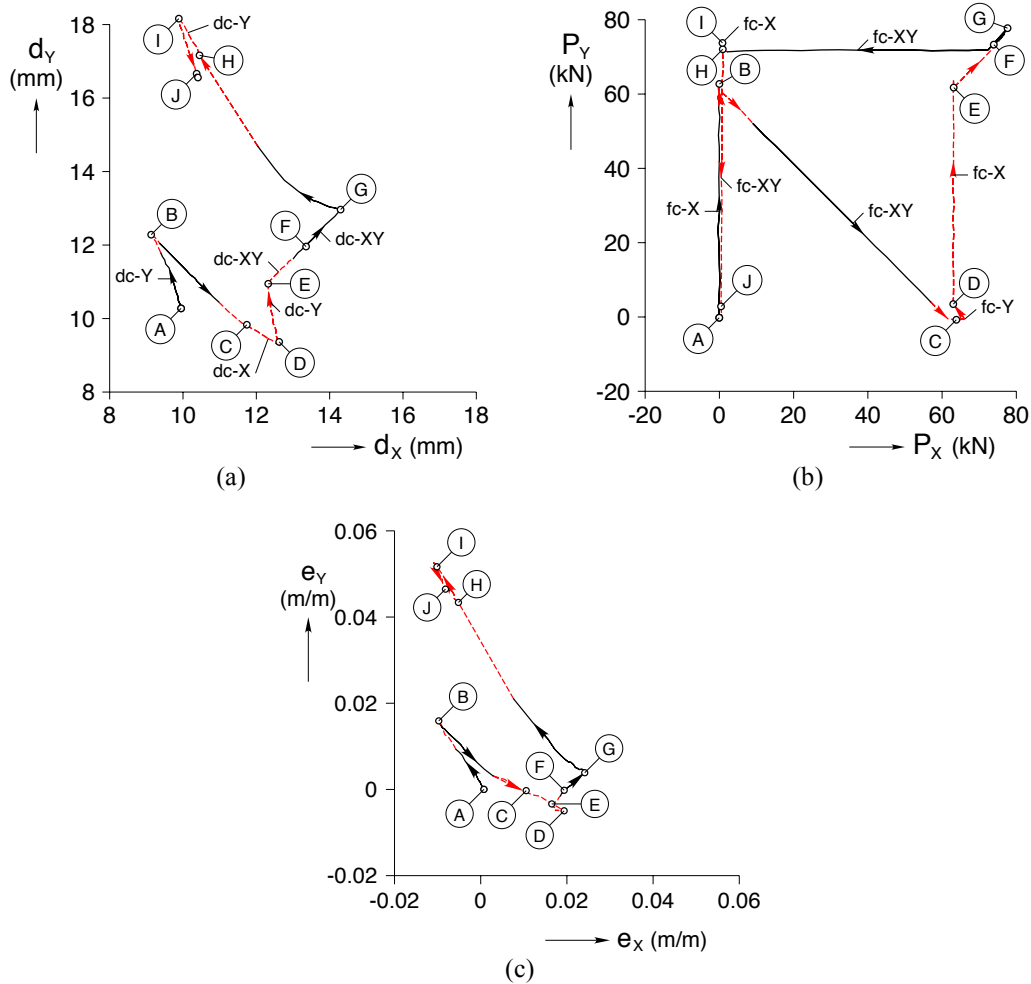


Fig. 5 Results for Example 2 (a) displacement, d , (b) force, P , and (c) strain, e , along the specimen X and Y axes. Key points in the loading paths are labeled by letters A through J, and the progression is denoted by the arrow on each segment with red dashed lines when buckling is present. "dc" denotes displacement control and "fc" denotes force control, with suffix "X" is applied to the X-axis and "Y" if applied to the Y-axis. Uncertainties in displacement and force are on the order of the line thicknesses shown in (a) and (b), and in strain are ± 0.00014 m/m.

Similar to Example 1, the shape of the displacement and strain paths do not agree, this is especially true in the segments where buckling is present. Buckling occurred at three locations in the loading paths. For clarity dashed red lines (Fig. 5) are used for segments where the specimen was buckled. The first occurred near the end of segment A-B, and was a small (± 0.35 mm out-of-plane) "S" shaped buckle along the X-axis of the gauge section (Fig. 6a). During segment B-C this buckle is removed, but another larger buckle forms (± 1.75 mm out-of-plane) with the same shape along the Y-axis in the gauge section (Fig. 6b). This larger buckle remained through segments C-D and D-E, and was finally flattened by the end of segment E-F. The third and final buckle occurs at the end of segment G-H, and is another large "S" shaped buckle (± 2.25 mm out-of-plane) aligned again with the X-axis (Fig. 6c). Since the system was in force control and this buckle occurred near $P_x = 1$ kN, the buckling resulted in a sudden jump in displacement (Fig. 6a) and strain (Fig. 6c) during segment G-H that is barely visible in the force (Fig. 6b) near point H. This final buckling remained to the end of the test. The onset of each buckling event occurred when the force along one axis approached zero. One might expect the specimen design in Fig. 3 with a reinforced (thicker) area around the thinner gauge section could result in the some elastic compressive force being transferred thicker reinforced ring to the thinner gauge section along the axis being unloaded resulting in buckling. This is consistent with each buckle shape (Fig. 6) being along the axis that is approaching zero force (Fig. 5b).

Modeling is planned to verify this hypothesis. This may result in a specimen design that has an envelope of applicability that is limited in part by a no buckling restriction.

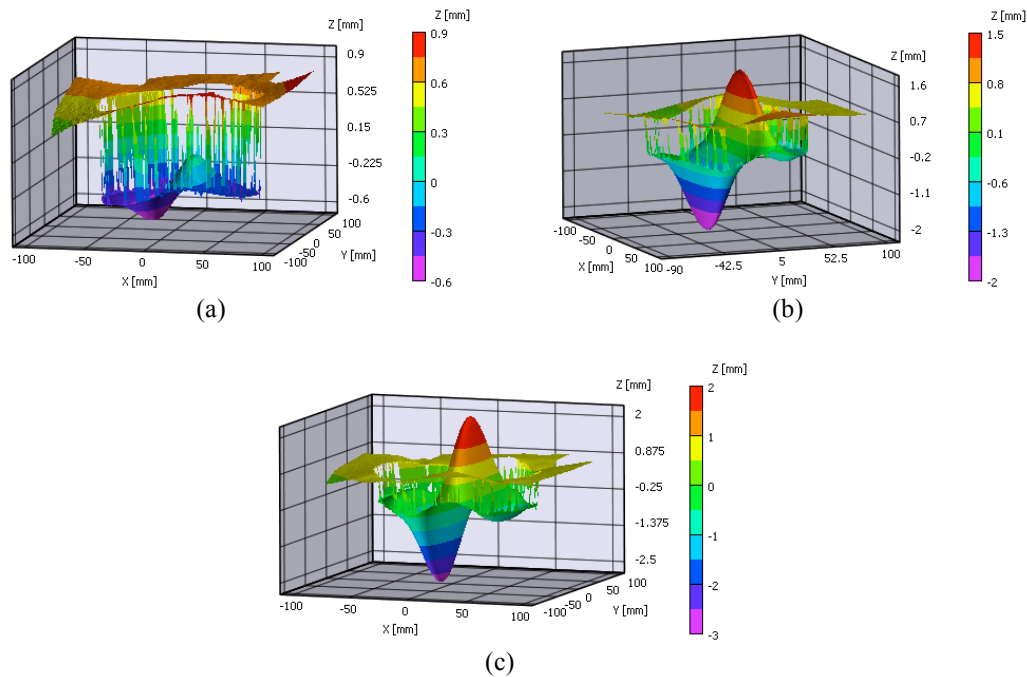


Fig. 6 3D-DIC height, Z, contour data in perspective plot showing buckling in Example 2 during segments (a) A-B, (b) C-D, and (c) G-H in Fig. 5.

Without 3D shape data, assessment of when the buckling occurred would be difficult, and quantifying the shape almost impossible. In addition to providing this 3D shape, the 3D-DIC system also has the advantage that its measurement of strain is not effected by the out-of-plane motion that may result in fictitious strains when using typical 2D strain mapping systems. The maximum strains achieved were $(\epsilon_x)_{\max} = 0.036$ and $(\epsilon_y)_{\max} = 0.054$, in the X and Y directions respectively. Although these are less than the expected forming limit strains for this material, the strain level is close to or above the strain limits seen for a specimen without a reduced thickness gauge section for a similar material [12].

5 Summary

Based on the testing performed and the results shown here the new biaxial testing facility at the National Institute of Standards and Technology Center for Automotive Lightweighting meets or exceeds its basic design specifications. Mechanical control has been demonstrated using various combinations of force and displacement control in both the elastic and plastic regimes. Full-field displacement and strain mapping was sufficient to track the specimen response, and is capable of tracking strain localizations and buckling phenomena. The specimen geometry used was not sufficient to obtain failure in the center of the gauge section, and will require further development. The geometry did show that it is very sensitive to potential buckling. Based on the results shown here, the system is capable of testing complex loading paths without unloading and re-machining the samples, assuming a specimen geometry can be found that does not buckle or result in premature failure at the edges of the gauge area.

Disclaimer

Certain commercial equipment, instruments, or materials are identified in this paper in order to specify the experimental procedure adequately. Such identification is not intended to imply recommendation or endorsement by the National Institute of Standards and Technology, nor is it intended to imply that the materials or equipment identified are necessarily the best available for the purpose.

References

- [1] F. Abu-Farha, L. G. Hector, Jr., and M. Khraisheh. Cruciform-shaped specimens for elevated temperature biaxial testing of lightweight materials. *JOM*, 61(8):48–56, AUG 2009.
- [2] D. Banabic. Anisotropy and formability of AA5182-0 aluminium alloy sheets. *CIRP Annals-Manufacturing Technology*, 53:219–222, 2004.
- [3] J. P. Boehler, S. Demmerle, and S. Koss. A new direct biaxial testing machine for anisotropic materials. *Experimental Mechanics*, 34:1–9, MAR 1994.
- [3] G. Ferron and A. Makinde. Design and development of a biaxial strength testing device. *Journal of Testing and Evaluation*, 16:253–256, MAY 1988.
- [4] T. Foecke, M. A. Iadicola, A. Lin, and S. W. Banovic. A method for direct measurement of multiaxial stress-strain curves in sheet metal. *Metallurgical and Materials Transactions A-Physical Metallurgy and Materials Science*, 38A:306–313, FEB 2007.
- [5] M. Geiger, W. Hussnätter, and M. Merklein. Specimen for a novel concept of the biaxial tension test. *Journal of Materials Processing Technology*, 167:177–183, AUG 30 2005.
- [6] D. E. Green, K. W. Neale, S. R. MacEwen, A. Makinde, and R. Perrin. Experimental investigation of the biaxial behaviour of an aluminum sheet. *International Journal of Plasticity*, 20:1677–1706, 2004.
- [7] E. Hoflerlin, A. Van Bael, P. Van Houtte, G. Steyaert, and C. De Mare. The design of a biaxial tensile test and its use for the validation of crystallographic yield loci. *Modeling and Simulation in Materials Science and Engineering*, 8:423–433, JUL 2000.
- [8] M. A. Iadicola, T. Foecke, and S. W. Banovic. Experimental observations of evolving yield loci in biaxially strained AA 5754-O. *International Journal of Plasticity*, 24(11):2084–2101, 2008.
- [9] S. Ikeda and T. Kuwabara. Work hardening behavior of if and low carbon steel sheets under biaxial tension. *Tetsu-to-Hagane Journal of the Iron and Steel Institute of Japan*, 90:34–40, DEC 2004.
- [10] T. Kuwabara, S. Ikeda, and K. Kuroda. Measurement and analysis of differential work hardening in cold-rolled steel sheet under biaxial tension. *Journal of Materials Processing Technology*, 80-81:517–523, AUG 1998.
- [11] Toshihiko Kuwabara, Albert van Bael, and Eiji Iizuka. Measurement and analysis of yield locus and work hardening characteristics of steel sheets with different r-values. *Acta Materialia*, 50:3717–3729, AUG 16 2002.
- [12] W. Müller and K. Pöhlant. New experiments for determining yield loci of sheet metal. *Journal of Materials Processing Technology*, 60:643–648, JUN 15 1996.
- [13] I.C. Noyan and J.B. Cohen. Residual Stress: Measurement by Diffraction and Interpretation. Springer-Verlag, 1987.
- [14] E. Shiratori and K. Ikegami. Experimental study of the subsequent yield surface by using cross-shaped specimens. *J. Mech. Phy. Solids*, 16:373–394, 1968.
- [15] Michael A. Sutton, Jean-José Orteu, and Hubert Schreier. Image Correlation for Shape, Motion and Deformation Measurements: Basic Concepts, Theory and Applications. Springer, 2009.
- [16] Yong Yu, Min Wan, Xiang-Dong Wu, and Xian-Bin Zhou. Design of a cruciform biaxial tensile specimen for limit strain analysis by fem. *Journal of Materials Processing Technology*, 123:67–70, APR 10 2002.